# Linear Dichroism in the X-ray Absorption Spectra of Linear *n*-Alkanes

**Juxia Fu and Stephen G. Urquhart***

*Department of Chemistry, University of Saskatchewan, 110 Science Place, Saskatoon, Saskatchewan, Canada S7N 5C9*

*Received: June 7, 2005; In Final Form: October 25, 2005*

The nature of the linear dichroism in the near-edge X-ray absorption fine structure (NEXAFS) spectra of linear *n*-alkanes is a matter of long-standing controversy. Linear dichroism in the carbon 1s → $\sigma^*_{C-C}$ transition has been interpreted within a building block model and a molecular orbital model, leading to two different descriptions for the angular dependence of this feature. When used for measurement of molecular orientation, the application of these two different models will lead to different results. We have explored the linear dichroism in the carbon 1s NEXAFS spectra of single crystals of the linear *n*-alkane hexacontane (*n*-$C_{60}H_{122}$). An analysis of the angular dependence in this spectrum shows that the transition dipole moment associated with the carbon 1s → $\sigma^*_{C-C}$ transition is oriented along the macromolecular chain axis, contradicting the predictions of the building block model. However, other transitions are observed in the $\sigma^*_{C-H}$ and the $\sigma^*_{C-C}$ bands that are orthogonal to the dominant transitions for each band. We also observe that radiation damage can be manifest in the form of molecular reorientation in highly ordered organic thin films.

## 1. Introduction

Linear dichroism (LD)[1−3] is the anisotropic absorption of linearly polarized electromagnetic radiation (EMR). LD spectroscopy is widely used to measure the orientation of biomaterials such as DNA,[4] proteins, polypeptides,[5] molecules adsorbed on surfaces,[6] self-assembled monolayers (SAMs),[7] Langmuir−Blodgett films,[8] rubbed polymers,[9] etc. Linear dichroism studies have been carried out by a wide variety of spectroscopic techniques, including surface-enhanced Raman spectroscopy (SERS),[10] attenuated total reflectance (ATR) spectroscopy,[11] infrared reflection absorption spectroscopy (IRRAS),[12] polarization modulation IRRAS spectroscopy,[12] near-edge X-ray absorption fine structure (NEXAFS) spectroscopy,[6,13] and NEXAFS spectromicroscopy.[13]

NEXAFS spectroscopy[6] is an ideal technique for probing the molecular orientation of organic materials because sharp core level excitations for carbon, nitrogen, oxygen, and fluorine occur in the soft X-ray region. Features in NEXAFS spectra are typically described in terms of one-electron transitions from core levels to unoccupied valence orbitals of $\pi^*$ and $\sigma^*$ symmetry, as well as Rydberg orbitals. These spectroscopic features can be used to identify the chemical composition of materials,[14−16] and their angle dependence can be used to measure the orientation of specific chemical moieties.[6,17−20]

The intensity of the NEXAFS resonances depends on the angle $\theta$ between the electric field vector of X-rays ($E$) and the direction of transition dipole moment (TDM, $\mu_{if}$) according to

$$I \propto |E\mu_{if}|^2 \propto \cos^2 \theta \quad (1)$$

where $\mu_{if}$ is the TDM for the one-electron transition from the initial state $\psi_i$ to the final state $\psi_f$ according to

$$\mu_{if} = \langle \psi_f | \mu | \psi_i \rangle \quad (2)$$

For example, for a 1s → $\pi^*$ transition, the TDM is perpendicular to the nodal plane of the $\pi$-bond. The transition intensity varies as $I = A \cos^2 \theta$, where $A$ describes the angle-integrated cross section and $\theta$ is as defined above.

In unsaturated molecules, the symmetry of the $\pi^*$ orbital creates an unambiguous relationship between the molecular frame and the TDM for the core → $\pi^*$ transition. Examples of the use of core → $\pi^*$ transitions for measurement of molecular orientation include polymer surfaces such as polyimides[9] and polystyrene[21] as well as many small molecules adsorbed on single-crystal surfaces.[6]

In saturated molecules such as *n*-alkanes, the character of the 1s → $\sigma^*$ transitions is controversial. As a starting point, there is a long-standing, perhaps never-ending controversy regarding the assignment of continuum features as $\sigma^*$ shape resonances. There is specific disagreement regarding the assignment of carbon 1s → $\sigma^*_{C-C}$ transitions in simple hydrocarbons such as ethane.[22] If, for the sake of discussion, we accept that continuum resonances in the carbon 1s NEXAFS spectra of *n*-alkanes can be considered as carbon 1s → $\sigma^*_{C-C}$ transitions, our next step is to consider their character. Unlike unsaturated molecules, the TDM vector for carbon 1s → $\sigma^*_{C-C}$ transitions cannot easily be projected onto the molecular frame. There are two common models for the $\sigma^*_{C-C}$ excited state: a building block (BB) model and a molecular orbital (MO) model. These models and the consequences of their selection will be discussed in detail below. If the continuum features observed in the NEXAFS spectra of *n*-alkanes cannot be properly described as carbon 1s → $\sigma^*_{C-C}$ transitions, measurement of their angle dependence remains very relevant. These spectroscopic features continue to be used for molecular orientation measurements, despite the ambiguity in their theoretical justification.

In the building block (BB) model proposed by Outka, Stöhr, and co-workers,[23] a molecule is viewed as an assembly of diatomic subunits or "building blocks". Linear alkanes are treated as the assembly of individual C−C "building blocks", and the angle dependence of the carbon 1s → $\sigma^*_{C-C}$ transition arises from the sum of the TDMs of the individual C−C building blocks, each TDM aligned along each C−C bond. Since this

* Corresponding author: email stephen.urquhart@usask.ca.

10.1021/jp053016q CCC: $30.25 
Published on Web 11/23/2005

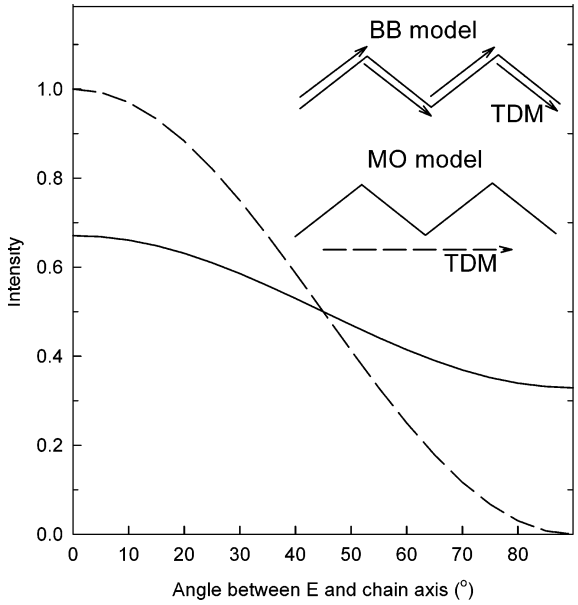


**Figure 1.** Relationship between the transition intensity and the angle between the transition dipole moment (TDM) and the electric field vector (*E*) for the carbon 1s NEXAFS spectra of linear alkanes, calculated within the building block (BB; —) and the molecular orbital (MO; − − −) models. The intensity scale is defined according to $I = A \cos^2 \theta$, where *A* describes the angle-integrated cross section ($A = 1$ in this figure).

model implicitly considers the electronic structure as the sum of the properties of *specific bonds between diatomic pairs*, this is in essence a *valence bond* description. In contrast to this BB model, Hähner et al.[7] have used a molecular orbital (MO) approach to consider the angle dependence of the C 1s NEXAFS spectra of *n*-alkanes. A molecular orbital can be delocalized over all or part of a molecule and not (necessarily) localized to a specific bond pair. Intuitively, we expect the $\sigma^*_{C-C}$ molecular orbital will be delocalized and aligned along the macromolecular axis of the *n*-alkane chain, rather than oriented along specific C−C bonds. As a consequence, the TDM of the carbon 1s → $\sigma^*_{C-C}$ transition should be aligned along the macromolecular axis in the MO model.

The predicted angle dependence for the carbon 1s → $\sigma^*_{C-C}$ transition in the NEXAFS spectrum of a linear *n*-alkane molecule based on the BB and the MO model is presented in Figure 1. This angle dependence is expressed as a function of the angle between the electric field vector (*E*) and the macromolecular chain axis of the *n*-alkane. The BB model is constructed by adding up the bond-specific contributions where the TDM is aligned along individual C−C bonds and the sum is derived by use of appropriate C−C−C bond angles.[24] The MO model assumes that the TDM is directed along the chain axis as a delocalized $\sigma^*_{C-C}$ molecular orbital.[7] Both models show that the intensity of the carbon 1s → $\sigma^*_{C-C}$ transition is at a maximum when the electric field vector is directed along the chain axis ($\theta = 0°$) and reaches a minimum when the electric field vector is perpendicular to the chain axis ($\theta = 90°$). The key difference between these models is the magnitude of the change. In the MO model, the intensity of the carbon 1s → $\sigma^*_{C-C}$ transition is predicted to go to zero at $\theta = 90°$, while this transition never goes to zero intensity in the BB model. The difference between models can be understood by considering the $\cos^2 \theta$ dependence for bond-specific contributions in the BB model. The MO and BB models are, of course, idealizations. This fact provides all the more reason precise experimental measurement of this linear dichroism is required, as these theoretical idealizations are the current basis of experimental methods for measuring molecular orientation.

Both the BB and the MO model have been widely used in the literature for the analysis of the orientation of alkanes such as alkanethiol and semifluorinated self-assembled monolayers absorbed on planar surfaces (see references 25 and 26). Here, the analysis is quite complex: the orientation of the spectroscopic TDM is described by a tilt angle ($\alpha$) relative to the surface normal and an azimuthal angle about the surface normal ($\phi$).[6] This azimuthal dependence will be averaged when multiple domains are present, such as in a typical self-assembled monolayer film.[6] The model relating the TDM to the molecular axis is then used to relate the spectroscopic angle dependence to the molecular orientation, by use of either the BB or the MO model. Several other factors can affect the magnitude of the linear dichroism. With any degree of azimuthal disorder, the intensity of the carbon 1s → $\sigma^*_{C-C}$ transition cannot go to zero—even in the MO description—unless the alkane chain is oriented exactly normal to the sample surface ($\alpha = 0$). Disorder in the chain conformation and photon ellipticity will also reduce the magnitude of the linear dichroism.

To understand the linear dichroism in the carbon 1s NEXAFS spectrum of linear alkanes, we need to experimentally characterize the absolute angle dependence of transitions found in its spectrum. For this, we require a highly ordered sample, preferably a single crystal. In particular, we wish to avoid the azimuthal averaging present in self-assembled monolayers. We also wish to measure the spectra of HC at all possible angles between the X-ray electric field vector and the molecular chain axis. In a typical angle-resolved NEXAFS measurement of a surface-absorbed molecule, the angle explored ranges between glancing (∼20°) and normal (90°) incidence. Several possible orientations of the *n*-alkane molecule in a *transmission geometry* are presented in Figure 2, where it is possible to rotate the sample azimuthally around the photon axis. When *n*-alkane chains are oriented normal to the sample surface, azimuthal rotation will not change the angle between the electric field vector and the alkane backbone axis (Figure 2a). However, if the alkane chains are induced to lie parallel to the sample surface (e.g., lateral orientation), azimuthal rotation can change the angle between the electric field vector and the alkane backbone axis, from 90° to 0°, as shown in Figure 2b. Consequently the angle dependence of the carbon 1s → $\sigma^*_{C-C}$ transition can be fully explored. We require a sample with the *n*-alkane chains laterally oriented in the plane of the sample surface.

This geometry requirement creates challenges for sample preparation. The simplest methods—solvent deposition of *n*-alkanes or the self-assembly of alkanethiols—result in films where the chains are oriented approximately normal to the sample surface, usually with some disorder. We have selected epitaxial growth[27−29] on crystalline surfaces to prepare samples where the *n*-alkane molecules are oriented in the sample plane, using methods developed for electron crystallography.[30,31] Our results show that the alkane molecules prepared in this manner are laterally oriented. By controlling the deposition conditions, we can prepare films with smaller or larger oriented domains.[32]

Scanning transmission X-ray microscopy (STXM) is used to acquire angle-resolved carbon 1s NEXAFS spectra of a well-ordered, laterally oriented hexacontane (HC) thin film at a range of azimuthal angles. In the STXM microscope, it is possible to rotate the sample azimuthally around the photon axis, change the X-ray polarization vector inclination (with an elliptically polarized undulator source), select specific sample areas, evaluate the presence of domains with different molecular orienta-

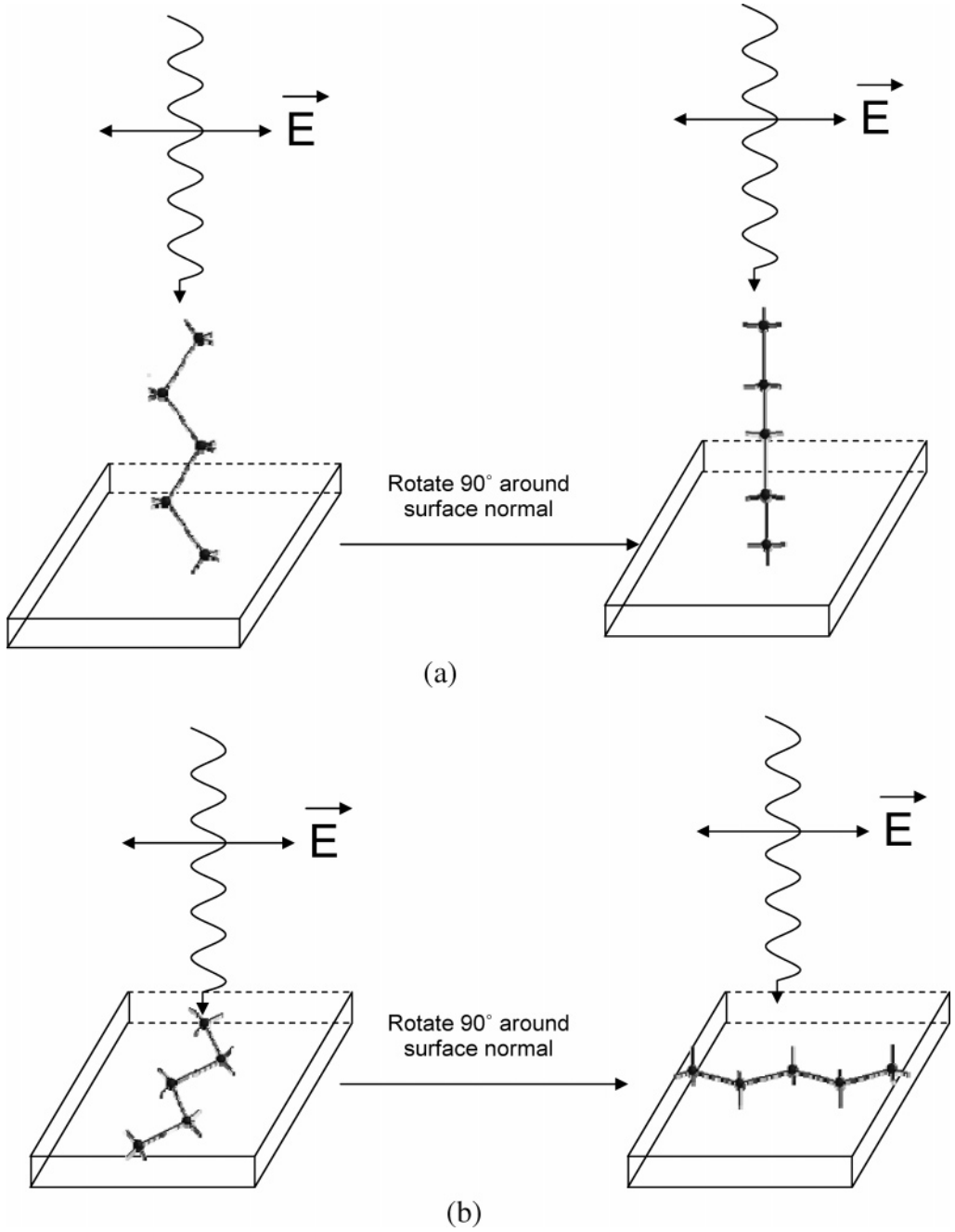


**Figure 2.** Schematic of alignment of linear alkane molecules relative to the substrate and the X-ray electric field vector. (a) Alkane molecule oriented normal to the substrate surface, electric field vector parallel to the substrate surface; (b) alkane molecules laterally oriented, electric field vector parallel to the substrate surface.

tions, and monitor the radiation dose. We have determined the absolute angle dependence of the transitions in this spectrum, and with these data considered the validity of the molecular orbital and the building block models for the angle dependence of the carbon 1s spectrum of *n*-alkanes.

## 2. Experimental Section

**2.1. Materials and Sample Preparation.** The linear alkane used in this study was hexacontane ($n$-$C_{60}H_{122}$, HC) (Sigma−Aldrich, 98% purity), used without further purification. The single-crystal NaCl substrates used were surplus Fourier transform infrared (FTIR) windows. Clean surfaces were prepared by cleaving the NaCl single crystal to expose a fresh (001) crystal plane. The substrates were placed in a high-vacuum chamber (Datacomp Scientific), and the evaporation was performed in a vacuum of $10^{-7}$ Torr from a resistively heated tungsten boat. The average thickness of the deposited films was measured with a quartz crystal microbalance. To have adequate absorption at the carbon 1s core edge, the sample thickness was maintained in the 100−150 nm range. A quartz light bulb heater and a thermocouple were used to control the temperature of the NaCl substrate during the HC deposition. After deposition, the NaCl substrate was dissolved in water (obtained from a Millipore water purification system, 18 MΩ) to separate the HC thin films from the substrate. The floating HC films were picked up on $Si_3N_4$ windows (Silson Ltd.) for X-ray microscopy experiments.

**2.2. NEXAFS Spectroscopy.** NEXAFS images and spectra were recorded at the Advanced Light Source (ALS) in Berkeley on two scanning transmission X-ray microscopes (STXM): the

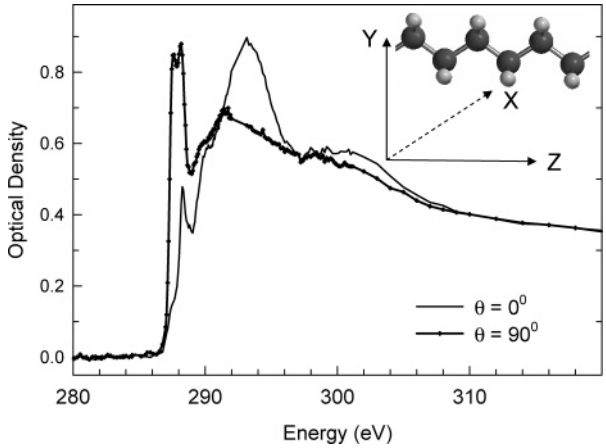


**Figure 3.** Carbon 1s NEXAFS spectra extracted from orthogonally oriented domains of HC, deposited on a freshly cleaved NaCl (001) surface with a room-temperature substrate temperature during evaporation. The spectrum (solid line) is extracted from domains that correspond to the angle $\theta = 0°$, that is, with the electric field vector oriented along the macromolecular backbone. The spectrum (line + data point) is extracted from domains that correspond to the angle $\theta = 90°$, that is, with the electric field vector oriented perpendicular to the macromolecular backbone. The molecular schematic illustrates the Cartesian coordinate conventions used in this paper.

polymer-STXM at beamline 5.3.2[33] and the molecular environmental sciences MES−STXM at beamline 11.0.2.[34] The polymer-STXM is on a bending magnet source, where we expect a photon polarization of 85−90% ellipticity, oriented in the horizontal plane. The MES−STXM is mounted on an elliptically polarized undulator (EPU) source, where the linear polarization can be inclined from horizontal to vertical.[35] The degree of linear polarization on this EPU has been measured to be 100% (+0/−1%) linearly polarized at several different inclinations.[36] The resolving power of the monochromator was 1900 for the 5.3.2 STXM beamline and 2500 for the 11.0.2 MES−STXM beamline.

All spectra were acquired in transmission mode and are reported as optical density versus energy (electronvolts). The optical density (OD), derived from the Beer−Lambert law, is obtained from $\mathrm{OD} = -\ln(I/I_0) = \mu\rho t$, where for a given X-ray energy $I_0$ is the incident flux (measured through a hole in the thin film), $I$ is the transmitted flux through the sample, $t$ is the sample thickness, $\mu$ is the mass absorption coefficient, and $\rho$ is the density. Since this sample is sensitive to radiation, special caution was taken when taking fine-scale images and spectra. To avoid the accumulation of radiation damage, each spectrum was acquired from a unique sample area.

## 3. Results and Discussion

**3.1. Carbon 1s NEXAFS Spectroscopy of Hexacontane.** Figure 3 presents carbon 1s NEXAFS spectra of a well-oriented HC thin film recorded at two different angles of the X-ray electric field vector with respect to the chain axis, along with the Cartesian coordinate system used for this molecule. The molecule HC belongs to the point group $C_{2h}$ and we use the following coordinate system to describe its orientation: All carbon atoms lie in the *yz* plane, the overall macromolecular axis is along the *z*-axis, and the $CH_2$ groups are parallel to the *xy* plane.

In Figure 3, the absence of a 285 eV feature demonstrates the low level of radiation damage in this typical exposure time. The band at ∼288 eV (below the ionization potential) is traditionally assigned as the carbon 1s → $\sigma^*_{C-H}$ band.[7,23,37] This band has the strongest intensity when the electric field vector is perpendicular to the alkane chain, that is, oriented in the $CH_2$ or *xy* plane (line with data points in Figure 3). In early electron energy loss spectra of gas-phase alkanes, this pre-edge band was assigned as 3s and 3p/$\pi^*(CH_2)$ transitions.[38] The similarity of the carbon 1s spectra of gaseous and condensed cyclic alkanes led Hitchcock et al.[39] to conclude that valence character was dominant in this mixed Rydberg/valence character state. When carbon 1s spectra of alkanes were recorded with much higher energy resolution, features were unambiguously assigned as Rydberg transitions,[35,40,41] although discussion of the degree of valence character is ongoing.[42,43] Curiously, Bagus et al.[25,44] concluded that pre-edge resonances in the carbon 1s spectra of *condensed* alkanes were predominantly Rydberg character even though it is generally expected that Rydberg states will be quenched in the solid state. Recent density functional theory (DFT) calculations of Weiss et al.[43] for *n*-octane show mixed valence−Rydberg character.

The resonances observed *above* the ionization threshold are often described within two variations of the shape resonance model. A *chemical orbital* model relates the character of the continuum resonances to the character of the unoccupied molecular orbitals,[45,46] in which these resonances are described as "core → $\sigma^*$ resonances" embedded in the continuum. This approach has the advantage of providing a direct relationship between the molecular structure and its spectrum through the familiar and predictive language of molecular orbital theory. Alternatively, continuum resonances are described by the trapping of the outgoing photoelectron by a potential barrier of the molecule;[47] this model is computationally studied with multiple scattering calculations.[48]

These shape resonances are frequently used in a building block approach, where the spectrum of a complex molecule is treated as the assembly of diatomic or pseudodiatomic fragments.[6] This building block model is the basis of the controversial bond length correlation method,[6,49] as well as the BB approach for linear dichroism described above.[6] Recently, Piancastelli[22] provided a critical review of these shape resonance interpretations. Multiple excitation, shake-up continuum, and shake-off continuum features are also considered as the origin of continuum features.

In the carbon 1s NEXAFS spectra of alkanes, there are two dominant features above the ionization potential that show angular dependence: a strong band at ∼293 eV and a weaker band at 301.1 eV. For convenience, we will use the traditional assignments of these transitions, that is, as carbon 1s → $\sigma^*_{C-C}$ and carbon 1s → $\sigma^*_{C-C'}$, respectively.[7]

**3.2. Preparation of Laterally Oriented HC Thin Films.** As outlined above, we require well-ordered *n*-alkane single crystals where the chains are oriented laterally in the sample plane and where the crystalline domains are large enough to permit the acquisition of several sequential spectra from the same domain. Radiation damage is a concern, and our sample area must be large enough to distribute the radiation dose from several sequential scans over a large enough sample volume to minimize the appearance of radiation damage. To estimate the sample area required, we performed a study of the radiation damage kinetics for HC following established procedures.[50,51] This procedure provides the critical dose: the radiation dose for the 1/e attenuation of the intensity of a particular transition or the corresponding increase in the intensity of a transition due to radiation damage. For HC, we found that the critical dose was 12 eV/nm$^3$ for the attenuation of the carbon 1s → $\sigma^*_{C-H}$ transition and 32 eV/nm$^3$ for the increase in the carbon

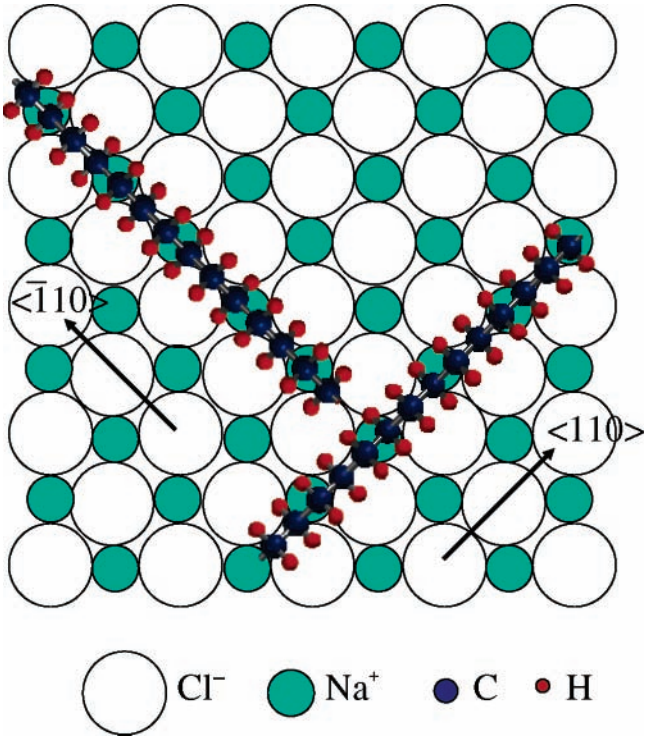


**Figure 4.** Expected epitaxial relationship between HC molecules and the NaCl (001) surface. The HC molecules (only 14 carbon atoms shown) are preferentially aligned along the two crystallographically equivalent ⟨110⟩ and ⟨$\bar{1}$10⟩ directions on the (001) surface.

1s → $\pi^*_{C=C}$ transition; the latter corresponds to the formation of C═C double bonds by radiation damage.[52] With a guideline of keeping the total radiation damage below the critical dose for the carbon 1s → $\sigma^*_{C-H}$ transition, we estimated that we would require an area of at least ∼170 $\mu m^2$ in order to acquire 10 spectra at different sample angles with dwell times and scan lengths typical for adequate statistics.

The expected epitaxial relationship between the NaCl (001) substrate and the HC molecules is shown in Figure 4. The high symmetry (cubic structure) and the ionic field force of NaCl induce the HC molecules to align on the NaCl (001) face along the crystallographically equivalent ⟨110⟩ and ⟨$\bar{1}$10⟩ directions.[31,53−55]

Oriented domains in samples prepared at room temperature are too small for reliable angle-resolved NEXAFS spectroscopy measurements,[32] particularly within the radiation damage limits described above. However, we found that we can modify the size of these domains by controlling the substrate temperature during film deposition.[30,31,56] Figure 5a presents an X-ray microscopy image recorded at 287.6 eV of an HC thin film evaporated onto freshly cleaved NaCl(001) where the substrate temperature was held at 45 °C during deposition. The image contrast is more uniform, consisting of an open area, a matrix (dark gray), and smaller dispersed domains (light gray). In Figure 5b, the image contrast inverts when the sample is rotated by ∼70° about the photon axis (note: this measurement was made with the bending magnet polymer STXM, where the X-ray electric field vector is horizontal). This sample consists of a majority phase aligned in one direction and a number of minority phases aligned at right angles to the majority phase. The morphological differences of this sample relative to the sample deposited at room temperature suggests that some additional energy is required to create larger crystals of HC by epitaxial growth.[30] For the sample prepared at room temperature, there is less thermal energy to promote molecular diffusion, and

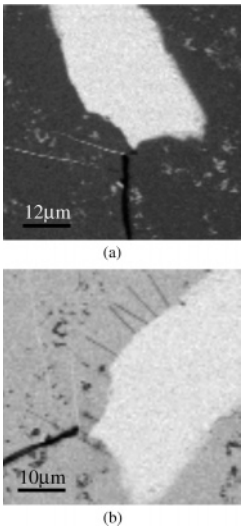


**Figure 5.** X-ray microscopic images of HC films' epitaxial growth onto a freshly cleaved NaCl (001) surface by thermal evaporation with substrate temperature of 45 °C during evaporation. These images were acquired with an X-ray energy of 287.6 eV. For image b, the sample has been rotated by 70°.

molecular movement on the substrate is limited. This leads to a higher effective density of nucleation sites and the formation of smaller crystallites. The sample deposited with a substrate temperature of 45 °C has large enough domains for our intended angle-resolved NEXAFS measurements.

**3.3. Measurement of the Angular Dependence of NEXAFS Spectra.** Angle-resolved NEXAFS spectra were measured on the bending magnet polymer-STXM (beamline 5.3.2) and elliptical polarized undulator (EPU) MES−STXM microscopes (beamline 11.0.2) at the Advanced Light Source. Since the bending magnet source is horizontally polarized, the sample must be rotated azimuthally around the photon axis by use of a rotation cell to measure the linear dichroism. Since the orientation of a particular domain is not initially known, measurements were made at a series of angles and the intensity of the carbon 1s → $\sigma^*_{C-H}$ band was monitored as a function of angle. The angles at which the intensity of the carbon 1s → $\sigma^*_{C-H}$ band reaches minimum and maximum were defined as $\theta = 0°$ and $\theta = 90°$, respectively. In the EPU measurements, the X-ray polarization can be changed from horizontal (EPU = 0°) to vertical (EPU = 90°) by shifting the EPU phase.[57] Nevertheless, it was still necessary to rotate the sample manually for the EPU measurements, as the 0−90° range of linear polarization inclination cannot cover the full angle range if the molecular domains are not perfectly aligned in the horizontal or vertical directions. Here, we only report the EPU data as we found a systematic attenuation in the intensity of stronger transitions in the bending magnet spectra. There are two potential origins for these differences: photon ellipticity and higher harmonic photon contamination. The increased ellipticity of a bending magnet source will decrease the *magnitude* of the linear dichroism, that is, decrease the intensity of the 293.5 eV carbon 1s → $\sigma^*_{C-C}$ transition and increase the intensity of the orthogonally oriented pre-edge carbon 1s → $\sigma^*_{C-H}$ transition, or vice versa. However, we found that the intensity of all strong features was attenuated in the bending magnet spectra, indicating that ellipticity alone is not responsible for the difference.

Higher harmonic contamination is a particular concern for the bending magnet STXM, which uses a spherical grating monochromator (SGM). The SGM monochromator produces significant second- and third-order harmonics, while the plane

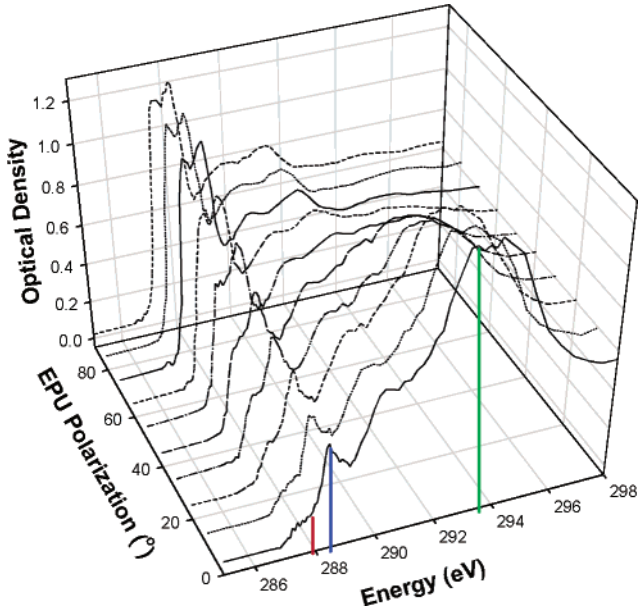


**Figure 6.** Carbon 1s NEXAFS spectra of an oriented HC thin film, prepared at a substrate temperature of 45 °C during evaporation, presented as a function of angle. These data were recorded by use of the MES−STXM microscope, by inclining the direction of the linear polarization and rotating the sample.

**TABLE 1: Energy and Full Width at Half Maximum of Transitions Optimized from the MGAUSS Fit of the Carbon 1s Spectra of HC**

| | | | | | | | | |
|---|---|---|---|---|---|---|---|---|
| peak position (eV) | 287.63 | 288.23 | 288.51 | 289.1 | 291.5 | 293.5 | 296.0 | 301.1 |
| fwhm (eV) | 0.51 | 0.68 | 0.54 | 2.28 | 1.31 | 3.56 | 5.97 | 7.90 |

grating monochromator of the MES−STXM beamline does not produce higher harmonics as efficiently. As higher harmonics will not be absorbed by the sample as efficiently as first-order photons, both the $I$ and $I_0$ signals will be artificially higher than for a pure radiation source, and the magnitude of the optical densities will be suppressed, as we observe.

Several causes of higher order contamination are specific to the STXM microscopes used for these experiments. The order sorting aperture should filter out higher harmonic photons, but small misalignments will lead to the transmission of these higher harmonics. These higher harmonics can be transmitted directly through the central stop of the zone plate focusing element if this element is not thick enough to not transmit at the energies of the harmonics.

Because the bending magnet spectra are systematically distorted, we will use only data acquired with the EPU source (MES−STXM) for the subsequent analysis. Proper consideration of these experimental factors is essential when NEXAFS spectra are acquired for linear dichroism studies.

Figure 6 presents the carbon 1s NEXAFS spectra of HC, recorded at 10 different angles, with the EPU source. We have used the MGAUSS program[58] to determine the angle dependence of features in our set of NEXAFS spectra. MGAUSS allows us to simultaneously fit the entire set of spectra to a common set of linked and independent parameters. In the angle-resolved spectra, we expect the *intensities* of specific features to vary but their *position* and *width* to remain invariant. Therefore, we constrained the energy and the width of spectroscopic features so they vary *identically* for all of the spectra in the simultaneous fit, while allowing the intensity of each feature to vary independently. To achieve the best fit of the 10 spectra recorded with different angles $\theta$, eight Gaussian curves

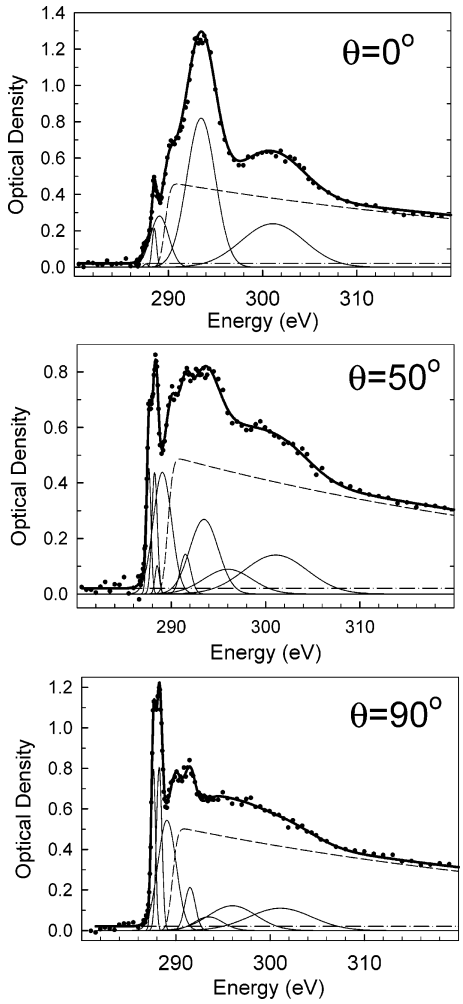


**Figure 7.** Fits of the carbon 1s NEXAFS spectra of HC films at three representative angles ($\theta$ = 0°, 50°, and 90°), fitted by MGAUSS program. These data were obtained by use of the elliptically polarized undulator (ALS beamline 11.0.2), for an HC sample deposited onto the NaCl (001) surface at a substrate temperature of 45 °C during evaporation. The line with symbols represents the experimental measured spectra; the thick solid line represents the best fitted spectra; thin solid lines, Gaussian peaks; dashed line, error step function; and dashed−dotted line, background.

were used to correspond to the spectral features and an error function (erf)[6] was used to model the ionization edge of carbon. The inflection point of the error function step was fixed at 289.7 eV, 1.0 eV lower than the ionization potential of gas phase of propane.[59] An orientation-independent background was also used. The parameters for the positions and shapes of the various NEXAFS resonances with angular-dependent intensity are listed in Table 1.

Figure 7 presents the angular dependence of carbon 1s NEXAFS spectra of HC films obtained on the MES−STXM at three representative angles, $\theta$ = 0°, 50°, and 90°. Figure 8 presents the optical density of each resonance as a function of angle ($\theta$) and $\cos^2\theta$. The $\cos^2\theta$ plot provides a diagnostic of experimental quality, as experimental linear dichroism data should have a $\cos^2\theta$ dependence (see eq 1). The $\cos^2\theta$ plots in Figure 8 are linear with the exception of the trace for the 293.5 eV feature. The linearity of all but one trace demonstrates that the experiment is free from major artifacts, and several reasons can be provided for the deviation of the one trace from linearity. This transition is the most intense continuum resonance, so it will be most sensitive to deficiencies in the functions used for the fit. We note that the continuum resonances are not

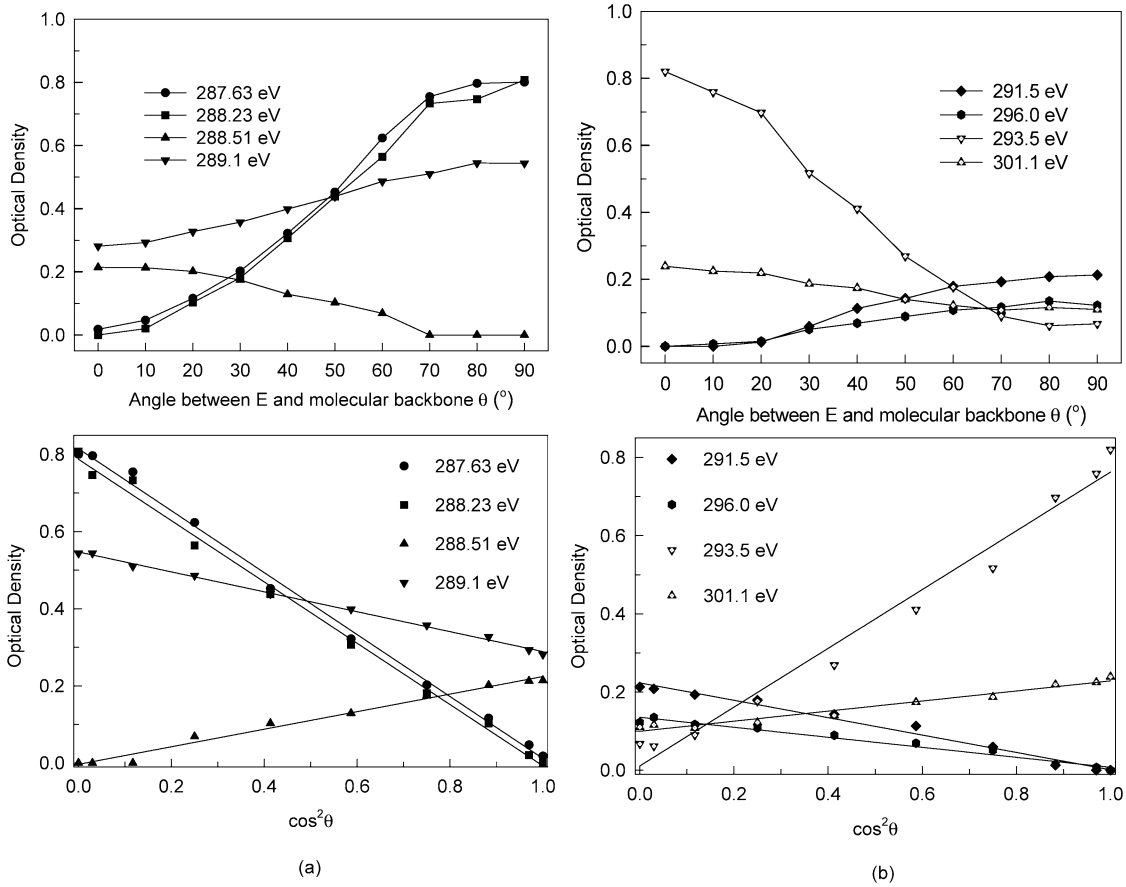


**Figure 8.** Optical density of resonances in the carbon 1s NEXAFS spectrum of HC as a function of angle $\theta$ and $\cos^2\theta$.

the symmetric Gaussians as used in the fit but rather are asymmetrically broadened by vibration.[6] Nevertheless, we fit these features with symmetric Gaussian functions as the addition of more functions to model this asymmetry would lead to overlap with other resonances and prevent us from tracking a specific resonance as a function of angle. This error will be highest when the 293.5 eV feature is most intense. However, this approach is a necessary compromise for the analysis of our data. When the 293.5 eV feature is at its minimum intensity, we find that radiation-induced molecular reorientation prevents us from observing zero intensity for this transition. This effect will be discussed below.

Four resonances were observed below the ionization potential in the spectral fit: at 287.63, 288.23, 288.51, and 289.1 eV (see Table 1). The resonances at 287.63 and 288.23 eV show a strong angle dependence with a maximum intensity when the electric field vector is oriented normal to the HC chain. The third resonance, at 288.51 eV, has an opposite angle dependence and a maximum intensity when the electric field vector is oriented along the macromolecular axis. The fourth Gaussian in the fit, at 289.1 eV, is unexpectedly broad and straddles the ionization potential. The inclusion of this Gaussian function is required for a good fit of the data, but given its character and the fact that we cannot observe this feature in the raw spectra, we do not assign it direct physical significance.

The first two transitions are considered to be carbon 1s $\rightarrow$ $\sigma^*_{C-H}$ transitions, as the TDM is oriented in the plane of the $CH_2$ group (e.g., the *xy* plane, orthogonal to the macromolecular backbone). The energy separation between these two resonances is 602 meV, in close agreement with the theoretical calculation value of 650 meV for *n*-octane.[43]

The intensity of the first two transitions goes nearly to zero when the electric field vector is aligned along the macromolecular backbone ($\theta = 0°$). This contrasts with the results of Hähner et al.,[7] in which the intensity of the C−H band decreases to approximately 30% of the maximum feature intensity. However, the data of Hähner et al. do not have adequate energy resolution to resolve the third transition at 288.51 eV. The failure to resolve this third, orthogonal transition in this fit results in the incorrect angular dependence observed by Hähner et al. Ironically, their C−H angle dependence looks like the hypothesized "building block" angle dependence (Figure 1), although this interpretation is not plausible for the planar $CH_2$ geometry. This observation demonstrates that adequate spectral resolution is required to properly characterize the angle dependence in these spectra. Conclusions regarding the electronic structure and molecular orientation based on insufficiently resolved spectra should be viewed with caution.

What is the spectroscopic character of the third pre-edge transition? We are reluctant to characterize this transition as a carbon 1s $\rightarrow$ $\sigma^*_{C-H}$ transition, as its TDM is oriented along the *z* axis, orthogonal to the $CH_2$ plane. We have considered that this transition might originate from the terminal $CH_3$ groups on the HC chain, as we expect a "C−H" component from the terminal $CH_3$ groups oriented along the macromolecular backbone direction. However, a stoichiometric calculation shows that this hypothesis is improbable. In HC, there are 6 C−H bonds in the terminal $CH_3$ groups versus 116 C−H bonds in methylene groups, that is, 5% of the C−H spectroscopic intensity will originate from the $CH_3$ group. Therefore, the intensity of the third peak is greater than would arise from stoichiometric considerations of the $CH_3$ group. Since this transition lacks the symmetry of a C−H resonance, a simple orbital picture of energy-separated C−H and C−C $\sigma^*$ bands does not hold. This C−H band has components in all three Cartesian directions.

We may be able to rationalize the character of this third transition by considering the role of Rydberg−valence mixing in the carbon 1s NEXAFS spectrum of HC. The carbon 1s → 3s transition and the carbon 1s → 3p Rydberg transition components directed in the *xy* plane can mix with states of $\sigma^*_{C-H}$ character.[42] Further, we expect that states of Rydberg character will be quenched in the solid state, so the transitions directed in the *xy* plane will be predominantly valence $\sigma^*_{C-H}$ character in condensed alkanes. In contrast, the 3p Rydberg component directed along the *z* axis cannot mix with states of $\sigma^*_{C-H}$ character and will remain as "pure Rydberg", which by symmetry cannot support mixing with states of $\sigma^*_{C-H}$ character. Such mixed and unmixed Rydberg states are observed in the gas-phase NEXAFS spectra of simple alkanes.[42]

Above the ionization potential, four resonances are resolved in the fit: at 291.5, 293.5, 296.0, and 301.1 eV (see Table 1 and Figure 8b). Each transition can be directly observed in at least a subset of the experimental data. The strong 293.5 and 301.1 eV transitions are assigned as carbon 1s → $\sigma^*_{C-C}$ and carbon 1s → $\sigma^*_{C-C'}$ transitions, respectively, by Stöhr et al.,[60] Hähner et al.[7] and Weiss et al.[43]

Our angle dependence data show that the intensity of the resonances at 293.5 and 301.1 eV has the strongest intensity when the electric field vector is aligned along the macromolecular or *z* axis. This is consistent with $\sigma^*_{C-C}$ character. In contrast, the resonances at 291.5 and 296.0 eV exhibit an opposite angular dependence, with maximum transition intensity when the electric field vector is normal to the macromolecular axis. These transitions lack the symmetry expected for a carbon 1s → $\sigma^*_{C-C}$ transition, in either the BB or MO model, and like the third (288.51 eV) transition in the C−H band, do not fit into a simplistic $\sigma^*_{C-C}$ orbital picture. The origin of these transitions is unclear.

Interestingly, it appears that features with a TDM along all three Cartesian components (*xy* plane, *z* axis) are observed in the $\sigma^*_{C-C}$ band just as in the $\sigma^*_{C-H}$ band. The observation of multiple, overlapping peaks in the $\sigma^*_{C-C}$ band with an orthogonal orientation dependence raises a caution about the use of these features for orientation analysis.

The carbon 1s → $\sigma^*_{C-C}$ transition at 293.5 eV exhibits the largest change with angle. This observation begs the question: does the angle dependence of this resonance follow the BB or the MO picture? We find that the ratio of the maximum to minimum optical density for this resonance is 13, approximately 6.5 times larger than the ratio based on the BB model. This result unambiguously excludes the BB model as a valid interpretation for this transition. On first glance, the MO model does not appear to be valid either, as this would require the intensity of the transition to go to zero at $\theta = 90°$. We will present several reasons why the transition might not go to zero: photon ellipticity, sample disorder, and radiation damage. Photon ellipticity can be excluded as the degree of linear polarization on the EPU beamline is 100% (+0/−1%). A small degree of disorder might be present in the as-deposited HC samples. Radiation may also cause a decrease in the degree of molecular alignment. Figure 9 presents the NEXAFS spectra of the oriented HC sample (from Figure 7, $\theta = 0°$) obtained after a small radiation dose (0.43 eV/nm$^3$) and a larger radiation dose (2.0 eV/nm$^3$). Comparison of these spectra shows that the optical density of the first resonance of carbon 1s → $\sigma^*_{C-H}$ (287.63 eV) *increased* with radiation dose, while the optical density of carbon 1s → $\sigma^*_{C-C}$ (293.5 eV) transition *decreased*. These *linear dichroism changes* indicates that the HC chains no longer have the same degree of alignment after the higher

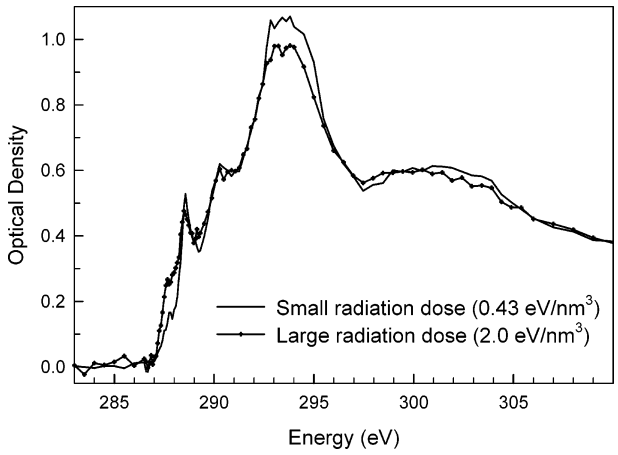


**Figure 9.** Carbon 1s NEXAFS spectra of HC, showing molecular reorientation induced by radiation dose.

radiation dose. These exposures are well below the critical doses required for *chemical* changes in HC, which leads to the loss of C−H bond (12 eV/nm$^3$) and formation of C=C bonds (32 eV/nm$^3$; see section 3.2). Indeed, loss of the C−H bond would attenuate the 288 eV region but have no effect on the carbon 1s → $\sigma^*_{C-C}$ transitions. However, since we see a clear linear dichroism effect—an *increase* in the carbon 1s → $\sigma^*_{C-H}$ transition and a *decrease* in the carbon 1s → $\sigma^*_{C-C}$ transition—these changes can be directly attributed to molecular reorientation.

The origin of this reorientation is a matter of speculation. One might consider that a temperature rise from the radiation exposure might induce molecular reorientation, although these radiation doses (2.0 eV/nm$^3$) are very low. A more likely scenario is that the radiation exposure causes fragmentation of the HC chains, where the fragments can reorient at ambient temperatures. Only one C−C bond needs to be broken to change HC ($n$-$C_{60}H_{122}$) into two $C_{30}$ fragments (or any other logical combination of fragment lengths). As the melting point of a $C_{30}$ chain (65∼67 °C) is ca. 30 °C below that of HC, chain fragmentation from radiation damage will lead to a distribution of shorter molecular chains, which can then undergo melting or reorientation at lower temperatures. The *chemical* effect of breaking *one bond* in a relatively long chain might not be visible spectroscopically, while the *physical* changes from the reduced melting point certainly can be. This observation is very unusual, as most radiation damage in NEXAFS spectroscopy is observed as chemical changes.[50,51] These changes are analogous to the loss in crystallinity observed with radiation exposure in electron crystallography measurements.

## 4. Conclusions

Linear dichroism in the carbon 1s NEXAFS spectra of *n*-hexacontane has been systematically explored. HC crystals with lateral orientation were prepared by epitaxial growth on a cleaved NaCl (001) surface.

This study shows that failure to properly resolve spectroscopic features with differing angle dependence will lead to an erroneous measurement of the angle dependence of the NEXAFS spectra, and from this, an incorrect description of the spectroscopic transition dipole moment. These errors are likely to lead to an inaccurate measurement of molecular orientation based on the angle-resolved NEXAFS spectra.

The analysis of angle-resolved NEXAFS spectra indicate that the transition dipole moment (TDM) for the carbon 1s → $\sigma^*_{C-C}$ transition at 293.5 eV in linear alkanes is oriented along the

macromolecular backbone, most closely corresponding to the molecular orbital model and explicitly excluding the building block model. However, transitions are observed in both the $\sigma^*_{C-C}$ and the $\sigma^*_{C-H}$ band that are oriented orthogonal to the primary transitions. These transitions do not fit into the conventional $\sigma^*_{C-H}$ and $\sigma^*_{C-C}$ band descriptions.

We observe that radiation damage can be manifest as a change in molecular orientation at a dose significantly below that for the observation of conventional X-ray radiation damage in the form of chemical bond breakage and formation.

**Acknowledgment.** This research was supported by the Natural Sciences and Engineering Research Council, the Canadian Foundation for Innovation, the Saskatchewan Synchrotron Institute, the University of Saskatchewan, and the Chemistry Department of the University of Saskatchewan. We are grateful to A. L. D. Kilcoyne and T. Tylizczak for help with the operation of the STXM microscopes at the ALS. The use of the ALS 5.3.2 STXM is supported by NSF DMR-9975694, DOE DE-FG02-98ER45737, Dow Chemical, an NSERC MFA, and the Canadian Foundation for Innovation. The ALS is supported by the Director, Office of Science, Office of Basic Energy Sciences, of the U.S. Department of Energy under Contract DE-AC03-76SF00098.

## References and Notes

(1) Norden, B. *Appl. Spectrosc. Rev.* **1978**, *14*, 157.
(2) Rodger, A.; Norden, B. *Circular dichroism and linear dichroism*; Oxford University Press: Oxford, U.K., 1997.
(3) Schellman, J.; Jensen, H. P. *Chem. Rev.* **1997**, *97*, 1359.
(4) Crain, J. N.; Kirakosian, A.; Lin, J. L.; Gu, Y. D.; Shah, R. R.; Abbott, N. L.; Himpsel, F. J. *J. Appl. Phys.* **2001**, *90*, 3291.
(5) Charney, E. *Q. Rev. Biophys.* **1988**, *25*, 1.
(6) Stöhr, J. *NEXAFS Spectroscopy*; Springer-Verlag: Berlin, Germany, 1992; Vol. 25.
(7) Hahner, G.; Kinzler, M.; Woll, C.; Grunze, M.; Scheller, M. K.; Cederbaum, L. S. *Phys. Rev. Lett.* **1991**, *67*, 851.
(8) Kinzler, M.; Schertel, A.; Hähner, G.; Wöll, C.; Grunze, M. *J. Chem. Phys.* **1994**, *100*, 7722.
(9) Samant, M. G.; Stöhr, J.; Brown, H. R.; Russell, T. P.; Sands, J. M.; Kumar, S. K. *Macromolecules* **1996**, *29*, 8334.
(10) Ianoul, A.; Fleury, F.; Duval, O.; Waigh, R.; Jardillier, J. C.; Alix, A. J. P.; Nabiev, I. *J. Phys. Chem. B* **1999**, *103*, 2008.
(11) Pelletier, I.; Laurin, I.; Buffeteau, T.; Desbat, B.; Pezolet, M. *Langmuir* **2003**, *19*, 1189.
(12) Pelletier, I.; Bourque, H.; Buffeteau, T.; Blaudez, D.; Desbat, B.; Pezolet, M. *J. Phys. Chem. B* **2002**, *106*, 1968.
(13) Ade, H.; Hsiao, B. *Science* **1993**, *262*, 1427.
(14) Urquhart, S. G.; Ade, H. *J. Phys. Chem. B* **2002**, *106*, 8531.
(15) Urquhart, S. G.; Hitchcock, A. P.; Smith, A. P.; Ade, H. W.; Lidy, W.; Rightor, E. G.; Mitchell, G. E. *J. Electron Spectrosc. Relat. Phenom.* **1999**, *100*, 119.
(16) Cooney, R. R.; Urquhart, S. G. *J. Phys. Chem. B* **2004**, *108*, 18185.
(17) Stöhr, J.; Outka, D. A. *Phys. Rev. B* **1987**, *36*, 7891.
(18) Stöhr, J.; Samant, M. G.; Cossy-Favre, A.; Diaz, J.; Momoi, Y.; Odahara, S.; Nagata, T. *Macromolecules* **1998**, *31*, 1942.
(19) Genzer, J.; Sivaniah, E.; Kramer, E. J.; Wang, J. G.; Xiang, M. L.; Char, K.; Ober, C. K.; Bubeck, R. A.; Fischer, D. A.; Graupe, M.; Colorado, R.; Shmakova, O. E.; Lee, T. R. *Macromolecules* **2000**, *33*, 6068.
(20) Genzer, J.; Sivaniah, E.; Kramer, E. J.; Wang, J. G.; Korner, H.; Char, K.; Ober, C. K.; DeKoven, B. M.; Bubeck, R. A.; Fischer, D. A.; Sambasivan, S. *Langmuir* **2000**, *16*, 1993.
(21) Fischer, D. A.; Mitchell, G. E.; Yeh, A. T.; Gland, J. L. *Appl. Surf. Sci.* **1998**, *133*.
(22) Piancastelli, M. N. *J. Electron Spectrosc. Relat. Phenom.* **1999**, *100*, 167.
(23) Outka, D. A.; Stohr, J.; Rabe, J. P.; Swalen, J. D.; Rotermund, H. H. *Phys. Rev. Lett.* **1987**, *59*, 1321.
(24) Hu, H.; Dorset, D. L. *Acta Crystallogr.* **1989**, *b45*, 283.
(25) Bagus, P. S.; Weiss, K.; Schertel, A.; Wöll, C.; Braun, W.; Hellwig, C.; Jung, C. *Chem. Phys. Lett.* **1996**, *248*, 129.
(26) Genzer, J.; Sivaniah, E.; Kramer, E. J.; Wang, J. G.; Korner, H.; Xiang, M. L.; Char, K.; Ober, C. K.; DeKoven, B. M.; Bubeck, R. A.; Chaudhury, M. K.; Sambasivan, S.; Fischer, D. A. *Macromolecules* **2000**, *33*, 1882.
(27) Pashley, D. W. *Adv. Phys.* **1965**, *14*, 327.
(28) Wellinghoff, S.; Rybnikar, F.; Baer, E. *J. Macromol. Sci.*—Phys. **1974**, *B10*, 1.
(29) Wittmann, J. C.; Lotz, B. *Prog. Polym. Sci.* **1990**, *15*, 909.
(30) Zhang, W. P.; Dorset, D. L. *J. Polym. Sci., Part B: Polym. Phys.* **1989**, *27*, 1433.
(31) Ueda, Y.; Ashida, M. *J. Electron Microsc.* **1980**, *29*, 38.
(32) Fu, J.; Urquhart, S. G. Manuscript in preparation, 2005.
(33) Kilcoyne, A. L. D.; Tyliszczak, T.; Steele, W. F.; Fakra, S.; Hitchcock, P.; Franck, K.; Anderson, E.; Harteneck, B.; Rightor, E. G.; Mitchell, G. E.; Hitchcock, A. P.; Yang, L.; Warwick, T.; Ade, H. *J. Synchrotron Radiat.* **2003**, *102*, 125.
(34) Tyliszczak, T.; Warwick, T.; Kilcoyne, A. L. D.; Fakra, S.; Shuh, D. K.; Yoon, T. H.; Brown, G. E.; Andrews, S.; Chembrolu, V.; Strachan, J.; Acremann, Y. *AIP Conf. Proc.* **2004**, *705*, 1356.
(35) Ma, Y.; Chen, C. T.; Meigs, G.; Randall, K.; Sette, F. *Phys. Rev. A* **1991**, *44*, 1848.
(36) Kortright, J. Personal communication.
(37) Haack, N.; Ceballos, G.; Wende, H.; Baberschke, K.; Arvanitis, D.; Ankudinov, A. L.; Rehr, J. J. *Phys. Rev. Lett.* **2000**, *84*, 614.
(38) Hitchcock, A. P.; Ishii, I. *J. Electron Spectrosc. Relat. Phenom.* **1987**, *42*.
(39) Hitchcock, A. P.; Newbury, D. C.; Ishii, I.; Stöhr, J.; Horsley, J. A.; Redwing, R. D.; Johnson, A. L.; Sette, F. *J. Chem. Phys.* **1986**, *85*, 4849.
(40) Remmers, G.; Domke, M.; Kaindl, G. *Phys. Rev. A* **1993**, *47*, 3085.
(41) Ueda, K.; Okunishi, M.; Chiba, H.; Shimizu, Y.; Ohmori, K.; Sato, Y.; Shigemasa, E.; Kosugi, N. *Chem. Phys. Lett.* **1995**, *236*, 311.
(42) Urquhart, S. G.; Gillies, R. *J. Phys. Chem. A* **2005**, *109*, 2151.
(43) Weiss, K.; Öström, H.; Triguero, L.; Ogasawara, H.; Garnier, M. G.; Pettersson, L. G. M.; Nilsson, A. *J. Electron Spectrosc. Relat. Phenom.* **2003**, *128*, 179.
(44) Weiss, K.; Bagus, P. S.; Woll, C. *J. Chem. Phys.* **1999**, *111*, 6834.
(45) Hitchcock, A. P.; Brion, C. E.; Van der Wiel, M. J. *J. Phys. B: Atom. Mol. Phys.* **1978**, *11*, 3245.
(46) Farren, R. E.; Sheehy, J. A.; Langhoff, P. W. *Chem. Phys. Lett.* **1991**, *177*, 307.
(47) Dehmer, J. L. *J. Chem. Phys.* **1972**, *56*, 4496.
(48) Thiel, W. *J. Electron Spectrosc.* **1983**, *31*, 151.
(49) Sette, F.; Stöhr, J.; Hitchcock, A. P. *Chem. Phys. Lett.* **1984**, *110*, 517.
(50) Rightor, E. G.; Hitchcock, A. P.; Ade, H.; Leapman, R. D.; Urquhart, S. G.; Smith, A. P.; Mitchell, G.; Fischer, D.; Shin, H. J.; Warwick, T. *J. Phys. Chem. B* **1997**, *101*, 1950.
(51) Coffey, T.; Urquhart, S. G.; Ade, H. *J. Electron Spectrosc. Relat. Phenom.* **2002**, *122*, 65.
(52) The radiation dose was calculated by dose = $(En_1n_2)/[V(\text{eff})]$, where $E$ is the energy at which the image was taken, $n_1$ is the number of absorbed photons per pixel, $n_2$ is the number of pixels, $V$ is the volume of the sample and eff is the efficiency of the detector; here we assume 30%.
(53) Ashida, M.; Ueda, Y.; Watanabe, T. *J. Polym. Sci.: Polym. Phys. Ed.* **1978**, *16*, 179.
(54) Mauritz, K. A.; Baer, E.; Hopfinger, A. J. *J. Polym. Sci.: Polym. Phys. Ed.* **1973**, *11*, 2185.
(55) Wittmann, J. C.; Hodge, A. M.; Lotz, B. *J. Polym. Sci.: Polym. Phys. Ed.* **1983**, *21*, 2495.
(56) Shimizu, H.; Tanigaki, N.; Nakayama, K. *Jpn. J. Appl. Phys.* **1995**, *34*, L701.
(57) Young, A. T.; Arenholz, E.; Marks, S.; Schlueter, R.; Steier, C.; Padmore, H. A.; Hitchcock, A. P.; Castner, D. G. *J. Synchrotron Radiat.* **2002**, *9*, 270.
(58) Tyliszczak, T. MGAUSS, McMaster University, Hamilton, Ontario, Canada.
(59) Siegbahn, K.; Nordling, C.; Johansson, G.; Hedman, J.; Heden, P. F.; Hamrin, K.; Gelius, U.; Bergmark, T.; Werme, L. O.; Manne, R.; Baer, Y. *ESCA applied to free molecules*; North-Holland Publishing Co.: Amsterdam, 1969.
(60) Stöhr, J.; Outka, D. A.; Baberschke, K.; Arvanitis, D.; Horsley, J. A. *Phys. Rev. B* **1987**, *36*, 2976.